AIAA JOURNAL
Vol. 48, No. 4, April 2010

Energy-Dissipating Composite Members with Progressive Failure: Impulsive Response and Experimental Verification

D. Stefan Dancila* and Erian A. Armanios†
University of Texas at Arlington, Arlington, Texas 76019

DOI: 10.2514/1.39786

An experimental investigation of response for tailored one-dimensional energy-dissipating composite members with progressive failure subject to quasi-static and impulsive tensile loading is presented. The tailoring concept relies upon a progressive failure sequence of redundant load paths of tailored strength and length to induce a yield-type response. In a prior publication the authors presented the concept development and analytical modeling of response under quasi-static loading. In this paper, an experimental verification is provided using a universal testing machine for members under quasi-static uniaxial loading. Furthermore, the model is extended to impulsive loading, and a custom-design drop test setup is developed to provide an experimental validation of analytical response. The results obtained confirm the hypothesized progressive failure sequence of redundant load paths, thereby validating the failure tailoring concept, as well as the accuracy and predictive power of the developed models of response in terms of both the number of partial failures induced for a given loading and the increased energy dissipation capability. Potential aerospace applications include snap-resistant tensile structures, for example space tethers, towing and cargo restraint lines, crashworthy helicopter troop seat stroke control straps, and aircraft emergency arrest gear.

Nomenclature

A	=	cross-sectional area
b	=	width
E	=	normal elastic modulus
F	=	logical constant false; nondimensional force; force
g	=	gravitational acceleration
i	=	running index
K	=	overall equivalent spring stiffness
k	=	equivalent spring stiffness
L	=	overall length
l	=	segment length; connector length
M	=	cart mass
m	=	mass
n	=	number of sublinks
O	=	Cartesian reference system origin
P	=	tip axial load; permutation set
p	=	primary
S	=	Boolean vector
s	=	secondary; Boolean vector
T	=	logical constant true
t	=	thickness; terminal; time variable
V	=	velocity
x	=	Cartesian coordinate
β	=	incline angle
δ	=	displacement; arrest distance
ε	=	strain
μ	=	shear modulus
ξ	=	nondimensional displacement
τ	=	time variable
ϕ	=	failure order permutation
χ	=	nondimensional acceleration
ψ	=	nondimensional velocity
ω	=	circular natural frequency

Subscripts

c	=	connector
f	=	failure
i	=	running index
j	=	running index
n	=	number of links
p	=	primary; running index
q	=	running index
s	=	secondary

Superscripts

c	=	connector
f	=	final
o	=	initial
p	=	primary; running index
q	=	running index
s	=	secondary; start
u	=	ultimate

Received 15 July 2008; revision received 3 March 2009; accepted for publication 29 June 2009.

*Associate Professor, Department of Mechanical and Aerospace Engineering, Box 19018, 500 West First Street, Woolf Hall 211. Senior Member AIAA.

†Professor and Chair, Department of Mechanical and Aerospace Engineering, Box 19018, 500 West First Street, Woolf Hall 211. Associate Fellow AIAA.

I. Introduction

A COMPOSITE failure tailoring concept for 1-D tensile members, appearing in Fig. 1, has been developed by the authors [1–3]. The concept relies upon a progressive failure sequence of redundant load paths of tailored strength and length to produce a yield-type response and increased energy dissipation compared with the conventional, untailored counterpart 1-D tensile members of identical length and cross-sectional area. Analytical models of response have been developed in [3] based upon a hypothesized progressive failure sequence. An experimental verification is presented in the current work providing validation of the tailored concept and verifying the predictive capability of the developed analytical models both with regard to the number of partial failures for a given loading, and with regard to the associated increase in energy dissipation. Furthermore, an investigation of response under impulsive loading has been undertaken entailing an extension of the quasi-static analytical model, as well as the development of a custom design drop test setup to validate the model analytical predictions.

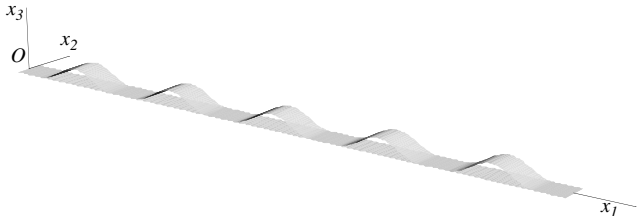

Fig. 1 Axonometric representation of a tailored composite member with $n = 5$.

II. Modeling of Response Under Quasi-Static Loading

A brief review of the tailored structural configuration and of the analytical modeling of response under quasi-static loading presented in [3] is provided in the following for the benefit of the reader.

The tailored structural configuration shown in Fig. 1 is formed by a continuous chain repetition of n identical composite link units such as the one shown in Fig. 2. The case of $n = 5$ is represented in Fig. 1.

The material is a flexible composite consisting of continuous high-performance fibers and an elastomeric matrix, which preserves the fibers' axial stiffness and strength while achieving a target level of bending compliance due to its reduced elastic moduli. This bending compliance characteristic is essential to the development of the technical solution investigated.

Each composite link is made of two segments of unequal length, joined at their ends over a connector region. The primary and secondary segment layers are made of unidirectional flexible composite material reinforced with continuous fibers oriented in the Ox_1x_3 plane of a Cartesian reference system $Ox_1x_2x_3$. Each link contains two subdomains, a connector domain and a segment domain. The connector domain, with a length l_c, has the primary and secondary layers running parallel to each other and bonded along the common interface. The segment domain, of length l_p, is characterized by a primary layer that remains flat while the secondary layer assumes a haversine-type shape, as shown in Fig. 2. The longitudinal modulus of elasticity of the material is E_{11}. The lengths, thickness, and cross-sectional areas of the primary and secondary segments are denoted by l_p and l_s, t_p and t_s, and A_p and A_s, respectively. The length of the connector regions is l_c. Subscripts p, s, and c denote primary, secondary, and connector quantities, respectively. The constraints $t_s > t_p$ and $l_s > l_p$ need to be met.

The combined thickness of the composite member t is given by

$$t = t_p + t_s$$

and the overall length L is related to the other model parameters by

$$L = (n+1)l_c + nl_p$$

The failure of the tailored composite member was hypothesized as a sequential, progressive failure of n primary segments, followed by the failure of one secondary segment. The order of failure is governed by the statistical distribution of failure loads among the primary segments and the secondary ones, respectively. The failure sequence determines the load redistribution within the tailored member during the $(n+1)$ response stages. The response of the models developed is governed by ten parameters divided into two groups, material property parameters and geometric parameters. The first group consists of the longitudinal axial modulus E_{11}, the longitudinal shear modulus μ_{12}, and the fiber failure strain ε_f^u. The second group consists of the number of links n, the length of the primary segments l_p, the length of secondary segments l_s, the connector length l_c, the thickness of the primary layer t_p, the thickness of the secondary layer t_s, and the width b.

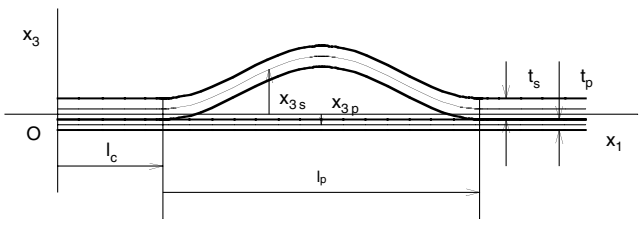

Fig. 2 Composite link.

The response of tailored composite members subject to a stroke-controlled loading was modeled by using a chain-of-springs analogy. Three models capturing the response of the tailored member to varying degrees of accuracy were developed.

Accurate-Connector-Stiffness Model: This analytical model accounts for the change in connector stiffness due to failure sequence and load redistribution. Because the failure sequence is stochastic, the model inherits this characteristic as well.

Define the equivalent spring stiffness for primary and secondary segments by

$$k_p = \frac{E_{11} b t_p}{l_p} \qquad k_s = \frac{E_{11} b t_s}{l_s}$$

Let P_n represent the set of all permutations of the sequence $\{1, 2, 3, \ldots, n\}$, with card $(P_n) = n!$, and let $\phi \in P_n$ be a randomly chosen member of this permutations set, interpreted as the failure sequence of the n links. Let s be an n-dimensional Boolean vector, the components of which are interpreted as current status of the n links. Initially

$$s_i = T, \quad (\forall)\ i \in \overline{1,n}$$

where T represents the Boolean value true and is interpreted as unfailed link state, and F represents the Boolean value false and is interpreted as failed link state.

Provided that at the end of every computational stage i, $1 \le i \le n$ a link status update is performed by $s_j = F$, where $j = \phi_i$, the set of equivalent stiffness of the tailored composite member can be consecutively computed by

$$K_i = \frac{1}{\sum_{p=1}^{n+1} \frac{1}{k_c^p} + \sum_{q=1}^{n} \frac{1}{k_l^q}} \qquad 1 \le i \le (n+1)$$

where

$$k_c^p = \begin{cases} k_c^{tp} & ((p=1) \wedge \neg s_1) \vee ((p=(n+1)) \wedge \neg s_n) \\ k_c^{ts} & ((p=1) \wedge s_1) \vee ((p=(n+1)) \wedge s_n) \\ k_c^{pp} & (2 \le p \le n) \wedge s_{p-1} \wedge s_p \\ k_c^{ps} & (2 \le p \le n) \wedge (s_{p-1} \forall\ s_p) \\ k_c^{ss} & (2 \le p \le n) \wedge \neg s_{p-1} \wedge \neg s_p \end{cases}$$

represents the equivalent stiffness of connector p and

$$k_l^q = \begin{cases} k_p & s_q \\ k_s & \neg s_q \end{cases}$$

represents the equivalent segment stiffness of link q.

Averaged-Connector-Stiffness Model: This model represents a simplified version of the first, obtained by assuming an averaged equivalent spring stiffness for the connectors. Consequently, the model becomes insensitive to failure sequence and deterministic.

An average value of 0.536 is assumed for the normalized connector stiffness. The connector stiffness can then be expressed by

$$k_c = 0.536 \frac{E_{11} b (t_p + t_s)}{l_c}$$

This constant value of connector stiffness leads to

$$K_i = \frac{k_p k_s k_c}{(n-i+1)k_s k_c + (i-1)k_p k_c + (n+1)k_p k_s}$$

Out of the ten controlling parameters, only nine are explicitly controlling the present model. The effect of the other parameter μ_{12} is

embedded in the constant used as an average value for the normalized connector stiffness.

Negligible-Connector Model: The simplest analytical model for the tailored composite member that still captures the essential elements of the response can be developed based upon the simplifying assumption $l_c \ll l_p$. This assumption represents the limiting case of either large l_p values corresponding to long members subdivided in few links by short connectors, or very small l_c values, made possible by high μ_{12} values.

Based upon this assumption, the connector is reduced to a point at which adjacent links connect and transfer load.

The equivalent spring stiffness of this model can be expressed as

$$K_i = \frac{k_p k_s}{(n-i+1)k_s + (i-1)k_p}$$

For each of the three models the load developed by the tailored member as a function of end displacement δ can be expressed as

$$P(\delta) = \sum_{i=1}^{n+1} P_i(\delta) \tag{1}$$

where

$$P_i = \begin{cases} K_i(\delta - (i-1)(l_s - l_p)) & \delta \in (\delta_i^s, \delta_i^u] \\ 0 & \delta \notin (\delta_i^s, \delta_i^u] \end{cases} \qquad 1 \le i \le (n+1)$$

and

$$\delta_i^s = \begin{cases} 0 & i = 1 \\ \max[\delta_{i-1}^u, (i-1)(l_s - l_p)] & 1 < i \le (n+1) \end{cases}$$

represents the end displacement at which the structure with $i-1$ primary failed links starts carrying load, whereas

$$\delta_i^u = \begin{cases} (i-1)(l_s - l_p) + \frac{P_p}{K_i} & i \ne (n+1) \\ (i-1)(l_s - l_p) + \frac{P_s}{K_i} & i = (n+1) \end{cases}$$

represents the end displacement at which the ith failure occurs.

A nondimensional form of load and tip displacement is given by

$$F = \frac{P}{E_{11} b (t_p + t_s) \varepsilon_f^u}$$

$$\xi = \frac{\delta}{L \varepsilon_f^u}$$

The quantities used as reference in the normalization process represent the load and tip displacement, respectively, of a conventional composite member with identical overall length, total cross-sectional area, and material properties.

III. Modeling of Response Under Impulsive Loading

The modeling of response under quasi-static loading is used to develop the tailored composite member response under impulsive loading. For all three models, the force vs displacement response is piecewise linear, with possibly zero-force segments interleaved between triangular/trapezoidal regions. It is shown in the following that the response under impulsive loading is piecewise sinusoidal, with possibly parabolic interleaved segments.

A. Force-Limited Spring-Mass System

As a preliminary step we are addressing the problem of the mass-spring system in Fig. 3. The mass m is supported by a linear spring of constant k and can move without friction along the incline of angle β. The original, unstretched length of the spring is l, and g denotes the gravitational acceleration. The spring is capable of generating a maximal force $F^{\max}$ before failure. At $t = \tau^0$ the system has the initial conditions $x = x^0$ and $V = V^0$.

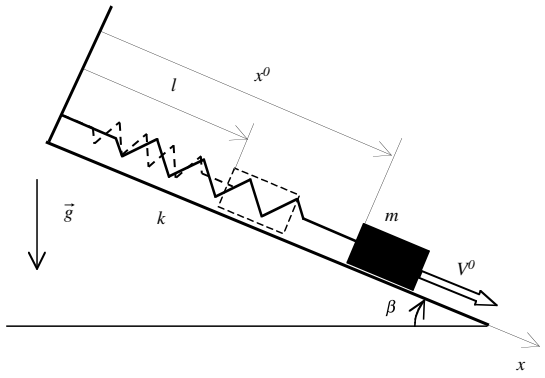

Fig. 3 Spring-mass system on incline.

The equation of motion can be written as

$$m\ddot{x} + kx = mg\sin(\beta) + kl \tag{2}$$

Denoting, as customary, $\omega = \sqrt{\frac{k}{m}}$ and taking into account the initial conditions stated, the solution can be expressed as

$$x(t) = \frac{V^0}{\omega}\sin(\omega(t-\tau^0)) + \left(x^0 - l - \frac{mg\sin(\beta)}{k}\right)\cos(\omega(t-\tau^0)) + l + \frac{mg\sin(\beta)}{k} \tag{3}$$

If the condition

$$\left| \frac{\frac{F^{\max} - mg\sin(\beta)}{k}}{\sqrt{\frac{(V^0)^2}{(\omega)^2} + (x^0 - l - \frac{mg\sin(\beta)}{k})^2}} \right| > 1 \tag{4}$$

is met then Eq. (3) is valid for all $t \ge \tau^0$ and the resulting response is an offset sinusoid. If, however, Eq. (4) is not satisfied, then the solution, Eq. (3), is only valid in the interval $\tau^0 \le t \le \tau^f$, where τ^f is given by

$$\tau^f = \tau^0 + \frac{1}{\omega}\arcsin\left(\frac{\frac{F^{\max} - mg\sin(\beta)}{k}}{\sqrt{\frac{(V^0)^2}{\omega^2} + (x^0 - l - \frac{mg\sin(\beta)}{k})^2}}\right) - \arctan\left(\frac{x^0 - l - \frac{mg\sin(\beta)}{k}}{\frac{V^0}{\omega}}\right) \tag{5}$$

In this case, at $t = \tau^f$ the spring fails. Subsequently, the equation of motion degenerates to

$$m\ddot{x} = mg\sin(\beta) \tag{6}$$

with the parabolic solution

$$\tilde{x}(t) = \frac{g\sin(\beta)}{2}(t-\tau^f)^2 + \dot{x}(\tau^f)(t-\tau^f) + x(\tau^f) \tag{7}$$

applicable for $t \ge \tau^f$.

B. Response of Tailored Composite Member

The load versus displacement response of tailored composite members is given by Eq. (1), and is piecewise linear. If, for any i, $1 < i \le (n+1)$ the inequality $\delta_{i-1}^u < \delta_i^s$ is met, where δ_i^u represents the ultimate end displacement of the structure after i partial failures and δ_i^s represents the end displacement at which the structure starts carrying load after i partial failures, then the response contains a zero-load segment for $\delta_{i-1}^u < \delta \le \delta_i^s$. The difference between the three models proposed for response under quasi-static loading consists in the method used to compute the stiffnesses K_i, and the corresponding values of δ_i^s and δ_i^u. The model extension developed in the following does equally apply to all three models.

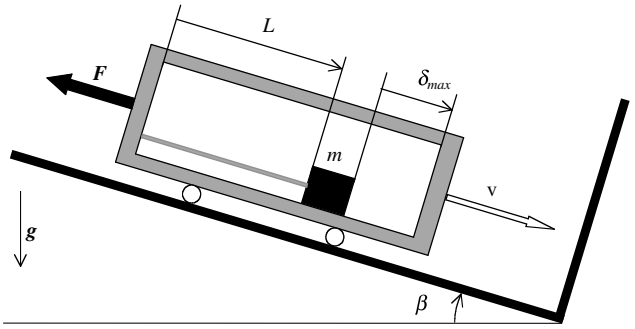

Fig. 4 Spring-mass system on incline.

Let us now consider the system in Fig. 4, with the restraint member replaced by a tailored structure. Subsequent to impact, the equation of motion for the payload mass can be expressed by

$$m\ddot{\delta} = mg\sin(\beta) - P(\delta) \tag{8}$$

where $P(\delta)$ is given by Eq. (1). Let us introduce the transformation of coordinates

$$x = L + \delta \tag{9}$$

and recognize that for $1 \le i \le (n+1)$ the zero-load length of the tailored member increases progressively as expressed by

$$L_i = L + (i-1)(l_s - l_p) \tag{10}$$

Then, the equation of motion Eq. (8) can be transformed into the set of differential equations

$$m\ddot{x} + K_i x = mg\sin(\beta) + K_i L_i \qquad 1 \le i \le (n+1)$$
$$x \in (L + \delta_i^s, L + \delta_i^u] \tag{11}$$

supplemented for every $i > 1$ such that $\delta_{i-1}^u < \delta_i^s$ by the degenerate form

$$m\ddot{x} = mg\sin(\beta) \qquad x \in (L + \delta_{i-1}^u, L + \delta_i^s] \tag{12}$$

Because the definition intervals are disjoint, for any given value of the coordinate x only one equation, corresponding to one particular index i in Eq. (11) or Eq. (12), is active. As the system switches from one interval to the following one, the final conditions at that point become initial conditions for subsequent motion. This indicates that the motion of the system can be obtained by sequentially solving Eqs. (11) and (12), through the following procedure.

Denoting $\omega_i = \sqrt{\frac{K_i}{m}}$ and assuming initial conditions x_i^0 and V_i^0, the generalized solution to Eqs. (11) can be expressed as

$$x_i(t) = \frac{V_i^0}{\omega_i}\sin(\omega_i(t-\tau_i^0)) + \left(x_i^0 - L_i - \frac{mg\sin(\beta)}{K_i}\right)\cos(\omega_i(t-\tau_i^0)) + L_i + \frac{mg\sin(\beta)}{K_i} \tag{13}$$

If at any stage i, the condition

$$\left|\frac{\frac{F_i^{\max} - mg\sin(\beta)}{K_i}}{\sqrt{\frac{(V_i^0)^2}{(\omega_i)^2} + (x_i^0 - L_i - \frac{mg\sin(\beta)}{K_i})^2}}\right| > 1 \tag{14}$$

is met, where

$$F_i^{\max} = \begin{cases} P_p & 1 \le i \le n \\ P_s & i = (n+1) \end{cases}$$

then Eq. (13) is valid for all $t \ge \tau_i^0$. If, however, Eq. (14) is not satisfied, then the solution, Eq. (13), is only valid in the interval $\tau_i^0 \le t \le \tau_i^f$, where τ_i^f is given by

$$\tau_i^f = \tau_i^f + \frac{1}{\omega_i}\arcsin\left(\frac{\frac{F_i^{\max} - mg\sin(\beta)}{K_i}}{\sqrt{\frac{(V_i^0)^2}{\omega_i^2} + (x_i^0 - L_i - \frac{mg\sin(\beta)}{K_i})^2}}\right) - \arctan\left(\frac{x_i^0 - L_i - \frac{mg\sin(\beta)}{K_i}}{\frac{V_i^0}{\omega_i}}\right) \tag{15}$$

In this case, at $t = \tau_i^f$ an ith segment fails. Subsequently, if

$$\delta_i^u < \delta_{i+1}^s \tag{16}$$

the solution to Eq. (12) is required and can be expressed as

$$\tilde{x}_i(t) = \frac{g\sin(\beta)}{2}(t - \tau_i^f)^2 + \dot{x}_i(\tau_i^f)(t - \tau_i^f) + x_i(\tau_i^f) \tag{17}$$

applicable for $\tau_i^f < t \le \tilde{\tau}_i^f$, where $\tilde{\tau}_i^f$ is the solution to

$$\tilde{x}_i(\tilde{\tau}_i^f) = L + \delta_{i+1}^s \tag{18}$$

The solution procedure follows. The first step consists in the determination of the initial conditions for the process. The velocity at the time of impact is given as V, therefore, $V_1^0 = V$. The initial position in the case of the system in Fig. 4 can be expressed as $x_1^0 = \frac{Fm}{K_1(M+m)}$. It is apparent that the effect of the applied force F is a preload in the tailored member, leading to an initial stretch present before impact. Finally, one can assume $\tau_1^0 = 0$ as the initial time.

Iterating from $i = 1$ to $(n+1)$, at every stage i Eq. (14) should be used first. If the condition in Eq. (16) is met then the current stage is the last one in the response sequence, Eq. (13) should be used for all subsequent time and the iteration process should be interrupted. Otherwise, the current stage will end with a segment failure, at a time given by Eq. (15). Using Eq. (13) one can compute the final conditions, corresponding to that time. If condition Eq. (16) is met, then the failure will be followed by a motion under the effect of inertia and gravity alone until load starts being applied again at a time given by Eq. (18). The final conditions for motion under Eq. (13) represent the initial conditions for motion under Eq. (17). In turn, the final conditions of this motion become the initial conditions at stage $(i+1)$. If, however, condition Eq. (16) is not met, then the end conditions under Eq. (13) are the ones to become the initial conditions at stage $(i+1)$.

The procedure was implemented as a Mathematica® notebook with calculations based upon each of the methods used for the stiffnesses K_i, respectively, and the corresponding values of δ_i^s and δ_i^u. Because the model response is, however, qualitatively similar in all three cases, only the accurate-connector-model is used, for illustration purposes, in the following.

An arrest problem is modeled by Fig. 4, for the basic composite tailored member configuration in Table 1. The problem is further characterized by $m = 100$ kg, $V = 3$ m/s, $F = 0$, and $\beta = \frac{\pi}{2}$, corresponding to the case of initial free vertical fall. The velocity is nondimensionalized by its initial value

$$\psi = \frac{\dot{x}}{V} \tag{19}$$

Table 1 Basic configuration parameter values

Property	Value
E_{11}	58.01 GPa
μ_{12}	5.24 MPa
ε_f^u	0.04
n	10
t_p	1.524×10^{-4} m
t_s	3.048×10^{-4} m
l_p	38.1×10^{-3} m
l_s	45.7×10^{-3} m
l_c	38.1×10^{-3} m
b	25.4×10^{-3} m

and the acceleration by the value of the gravitational acceleration g

$$\chi = \frac{\ddot{x}}{g} \tag{20}$$

Assuming a failure sequence given by the randomly chosen permutation $\phi = \{8, 9, 5, 4, 10, 3, 7, 6, 1, 2\}$, the corresponding response is shown in Figs. 5–8. For comparison, the response of a conventional composite material structure of identical length, total cross-sectional area, and material properties to the same arrest problem is also shown in these figures.

The history of force developed during the arrest sequence appears in Fig. 5. It can be seen that the conventional composite member develops a force that is three times higher than that of the tailored member but fails to arrest the body. By contrast, the tailored composite member develops a flattened response and completely arrests the moving body through a progressive failure of nine of its ten primary segments.

The corresponding displacement history is illustrated in Fig. 6. It can be seen that the response of the conventional member is initially characterized by smaller displacements. However, after failure occurs the displacement starts growing rapidly following a parabolic law of the type given in Eq. (17). In the case of the tailored composite the displacement is limited, indicating a complete arrest.

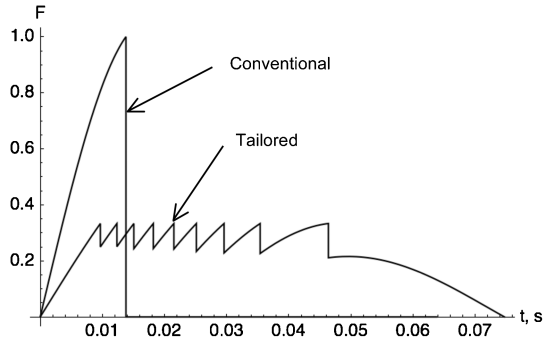

Fig. 5 Normalized force response.

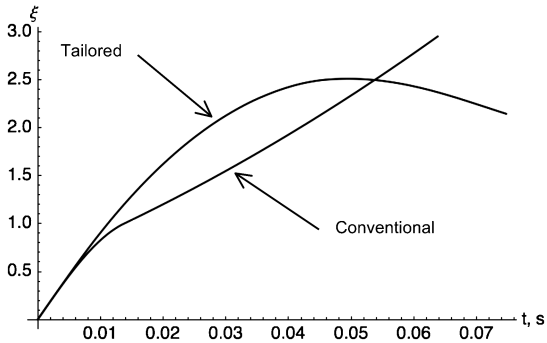

Fig. 6 Normalized displacement response.

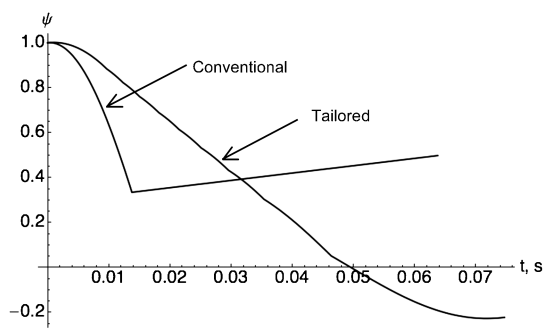

Fig. 7 Normalized velocity response.

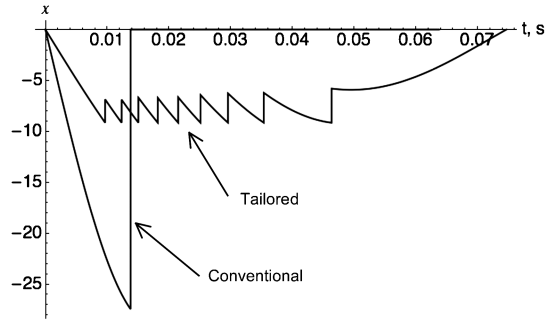

Fig. 8 Normalized acceleration response.

The comparison of velocity history appears in Fig. 7. The conventional composite member reduces the velocity of the mass to approximately 35% of the initial value. Failure of this member, however, causes the velocity to start increasing beyond this point in a linear manner, corresponding to subsequent free fall of the body. By contrast, the tailored composite member is successful in progressively reducing the velocity of the mass to zero.

Finally, the inertial loading on the payload mass during the arrest sequence is shown in Fig. 8. It can be noticed that Fig. 8 can be obtained from Fig. 5 through a reflection and a scaling along the ordinate axis. The use of the conventional composite member leads to high deceleration levels in excess of 25 g, while failing to provide the required arrest. By contrast, the use of the tailored composite member produces deceleration levels of less than 10 g and a complete arrest. This response clearly illustrates the benefits of the developed tailoring concept.

IV. Experimental Verification

A. Material System

A material system consisting of a pressure-sensitive rubber adhesive reinforced with glass fibers was selected for the present investigation due to availability and low cost. The prepreg, commercially available as Scotch 898 High Performance Filament Tape, has a thickness of 152.4 μm and a width of 25.4 mm, and is manufactured by the 3M Company. It uses Owens Corning ECG 150 E-glass yarns embedded in an uncharacterized rubber resin and attached to a thin, 25.4 μm Scotchpar polyester backing tape. The fiber volume fraction is estimated as equal to 0.145, with the effect of the backing tape included. The glass fiber characteristics are given in Table 2.

Based upon the fiber volume fraction, the longitudinal Young's modulus of the composite E_{11} is estimated at 10.0 GPa, based upon a rule of mixture model [4], a value confirmed experimentally.

Observations showed that the pressure-sensitive rubber resin matrix is characterized by a viscoelastic response. A quantitative matrix material characterization was, however, not available, due to the fact that the information is not disclosed by the manufacturer and the matrix material was not separately available for testing.

Because the properties of the matrix material were not known, a calculation of minimum connector length was not possible. A conservative connector length that avoids connector failure in the specimen configurations investigated, under the loading conditions applied, was established experimentally during preliminary testing.

An average failure load of 1840 N per filament tape ply was experimentally obtained, versus the value of 1687.2 N published by the manufacturer. The variance is attributed primarily to differences in loading rates.

B. Specimen Configurations

Tailored composite members with the characteristics shown in Table 3 were manufactured and tested. The selected thickness values correspond to single ply primary segments and double ply secondary segments and were chosen based upon practical considerations.

Table 2 Glass fiber characteristics

Property	Value
Young's modulus E_1	68.9 GPa
Poisson's ratio ν_1	0.22
Failure strain ε_f	0.047
Strength	3.44 GPa

Table 3 Specimen configurations

Property	Value
E_{11}	10.0 GPa
ε_f^u	0.047
n	3, 5, 7, 10
t_p	1.524×10^{-4} m
t_s	3.048×10^{-4} m
l_p	38.1×10^{-3} m
l_s	45.7×10^{-3} m
l_c	38.1×10^{-3} m
b	25.4×10^{-3} m

A connector length l_c of 38.1×10^{-3} m, or 1.5 in., was experimentally found to avoid connector shear failure for the loading cases investigated and was used for all specimens. A primary segment length l_p of 38.1×10^{-3} m, or 1.5 in., was also selected based upon manufacturing considerations, as well as a secondary segment length l_s equal to 45.7×10^{-3} m.

Preliminary testing showed that primary segment failure near connectors is detrimental and may trigger connector delaminations and premature failure. To prevent this, semicircular notches with a radius of 3 mm are placed on one side of each primary segment at equal distance from the connectors, effectively localizing the failure at that cross section. It is found through testing that the failure load of primary segments is reduced by approximately 19% to an average value of 1490 N. The application of notches is the simplified counterpart of manufacturing primary segments with a dog-bone shape.

Fig. 9 Quasi-static testing configuration, general view.

C. Quasi-Static Loading

1. Testing Configuration

A computer-controlled, universal hydraulic testing machine was used for testing of conventional and tailored composite specimens under quasi-static loading conditions. The testing software system allows the definition and use of testing procedures, which perform both test control and data acquisition functions. A custom testing procedure was written for the present testing program.

Figure 9 shows a general view of the testing configuration. A ten-link specimen is shown in Fig. 9 connected between the grips of the testing machine through two buckle-type attachments. A detailed view of the lower grip with the corresponding buckle attachment and the connected specimen is shown in Fig. 10. Also shown in Fig. 10 are the notches used to localize the primary segment failure.

A 45 mm/s displacement-control ramp is applied and the corresponding load and displacement data is automatically acquired, displayed, and logged.

2. Results and Discussion

A number of tailored composite members with 3, 5, 7, and 10 links and their respective conventional counterparts have been tested. Figure 11 shows a typical result, obtained for a 10-link tailored member and the corresponding untailored member. Figure 12 shows the analytically predicted nondimensional load vs tip displacement curve.

As a general observation, the measured response of the tailored composite member follows the predicted pattern of 10 primary segment failures followed by a secondary segment failure. The variability in primary segment failure load is at least in part due to the observed scatter in tape ply strength properties. The fact that the primary segment failure load is lower than the predicted value of 0.33 is due to the presence of notches, not accounted for in the analytical models. The failure load of a secondary segment is, as expected, close to 0.67. Measured nondimensional tip displacements appear to be somewhat larger than predicted, most likely due to the response of the matrix.

The response of the conventional composite member is characterized by a nondimensional failure load of 0.81 instead of the expected value of 1. In part, this is again attributed to variability of failure load for the tape ply and also to observed waviness in fiber geometry, also responsible for the nonlinear initial region of the response curve. The small difference in the nondimensional failure

Fig. 10 Quasi-static testing configuration, detail.

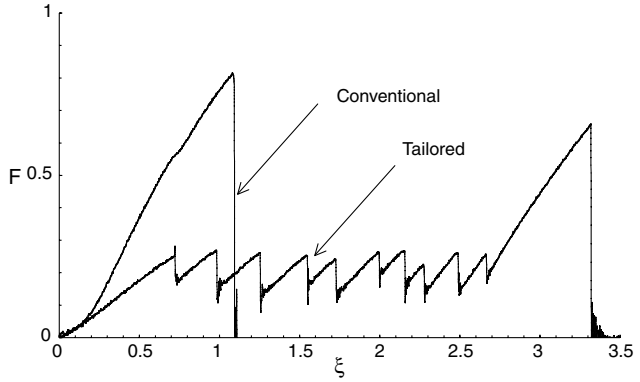

Fig. 11 Measured load vs tip displacement response, $n = 10$.

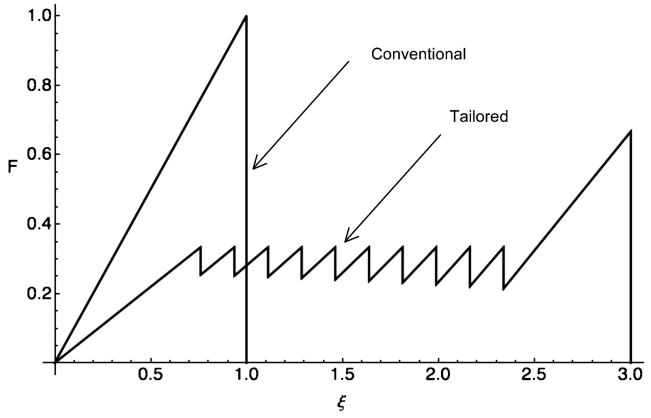

Fig. 12 Predicted load vs tip displacement response, $n = 10$.

tip displacement can be at least in part correlated with the initially nonlinear response.

The ratio of areas under the measured nondimensional response curves is 1.77, compared with the predicted value of 1.74, and confirms the increased energy dissipation capability of the tailored configuration compared with the conventional one.

It can be concluded that, within the limits of accuracy allowed by the material system used, the measured response shows good agreement with the predictions of the analytical models developed.

D. Impulsive Loading

1. Testing Configuration

The testing of tailored and conventional composite members under impulsive loading was accomplished by using a custom designed drop test stand, shown in Fig. 13. The stand is built upon the load frame of a four-column, screw-type testing machine and comprises an upper support, a vertically mobile cart incorporating a lead block, a rope lifting system equipped with an electromagnet, and instrumentation.

The upper support consists in steel rod is attached to the upper crosshead of the testing machine through a spherical joint. This connection allows the rod to orient the upper support along the direction of applied force, resulting in axial loading only. A buckle-type element, with a tailored composite specimen attached, is connected to the steel rod through a piezoelectric force link transducer. Part of the cart lifting system can also be seen in Fig. 13, represented by the chain support, attachment hook, locking pulley and rope.

The mobile cart consists of a horizontal C channel steel beam moving vertically between two diagonally opposed columns of the testing machine, guided by an assembly of four ball-bearing, low-friction rubber wheels at each end. A rectangular steel frame located underneath the C channel beam is housing a 24.5 kg lead block. A buckle-type element, with a tailored composite member attached to it, is bolted to the middle of the horizontal C channel bar. The lifting rope is connected to an electromagnet, which is used to lift and

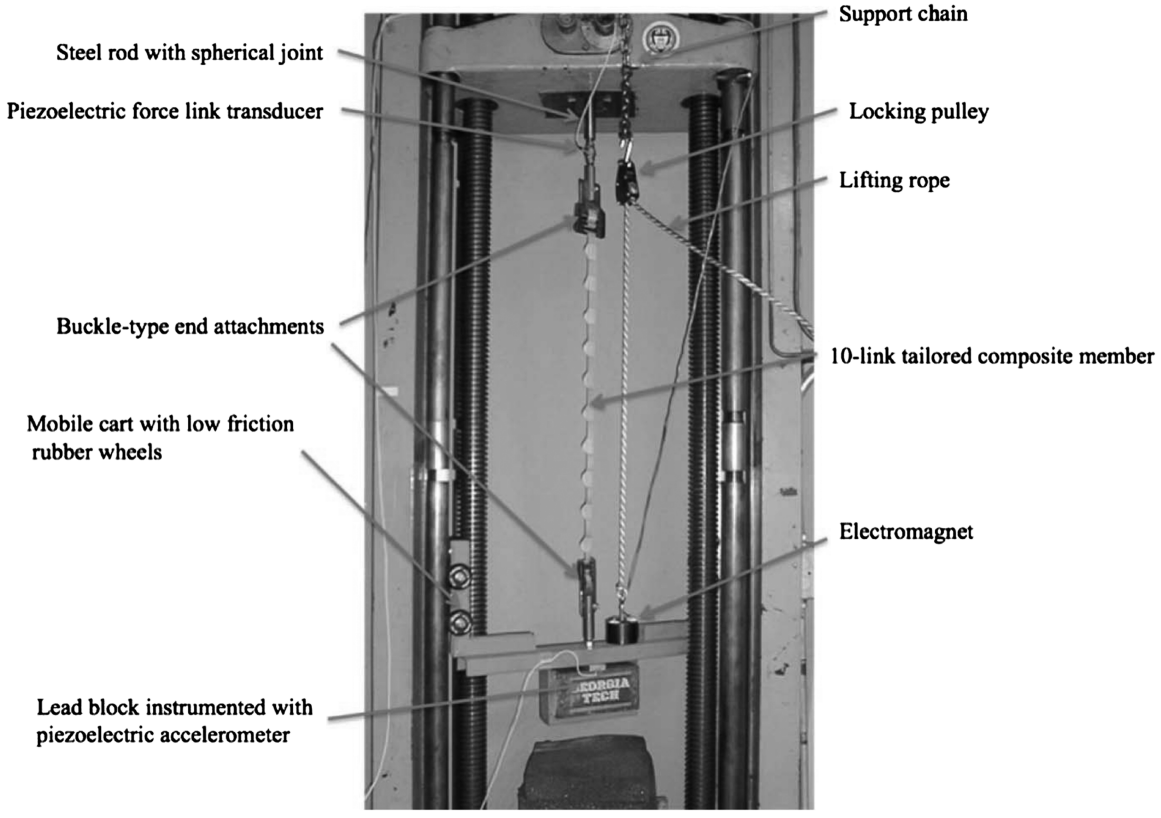

Fig. 13 Drop test stand and components.

release the cart. A piezoelectric accelerometer is attached to the side of the lead block. The total mass of the cart is 34 kg.

At the core of the instrumentation and control equipment setup is a laptop computer with an analog/digital input/output card. The control and data acquisition functions required by the testing program have been implemented by programming a set of custom virtual instruments using the graphical programming language G, available in LabVIEW. A digital oscilloscope, a voltage-and-current regulated source, two unit gain piezoelectric amplifiers with DC coupling, and a two-channel, analog filtering unit are also used. A buffered, solid-state relay is part of the setup. The force transducer, characterized by a sensitivity of 9.64×10^{-5} V/N, is connected to the DC coupled, unit gain amplifier and the amplifier output signal is directed to one input channel of the digital oscilloscope and to one analog input channel of the data acquisition card. When required, the signal can be acquired at a rate of 10,000 samples per second and stored. The test instrumentation and control are shown in Fig. 14.

Using one digital output channel connected to the solid-state relay, the testing procedure controls the current applied by the current regulated source to the electromagnet used in the cart lifting system. When a current is applied, the electromagnet is capable of a clamping force in excess of the cart weight, making it possible to lift the cart by using the rope. Subsequently, at the time when the cart is to be released, a switching of the solid-state relay causes the current to be interrupted and the cart drops under its own weight.

2. *Testing Procedure*

Figure 15 shows the testing system in a ready-for-drop configuration. The electromagnet is clamped on the cart and the rope and locking pulley are supporting the cart's weight. A tailored composite member is shown attached to the upper and lower buckles. Under the control of the testing procedure, the solid-state relay is switched off, causing the electromagnet to release. Simultaneously, the data acquisition process for the force and acceleration signals is started. The cart undergoes a free fall until the moment when the composite member becomes taut. Subsequently, the cart applies an impulsive load to the composite member and the force response history is acquired. Processing of the acquired signal through a low-pass digital filter removes the high-frequency noise. The final processing step consists of the scaling of the filtered signal to obtain the force history associated with the impulsive loading.

The velocity at which the impulsive loading is applied can be controlled through the cart free fall distance, and the amount of energy provided is determined by the combination of cart mass and cart velocity.

3. *Results and Discussion*

A number of tests have been conducted for several configurations of interest. In the following a set of typical results are presented, obtained for 10-link tailored members and their conventional counterparts, subject to the impulsive loading corresponding to cart drop distances of 0.178, 0.254, 0.381, and 0.635 m.

Case 1: The case of a cart drop distance of 0.178 m, or 7 in., corresponding to a speed of 1.867 m/s at the initiation of arrest, is presented first. The load history prediction for the tailored and conventional configurations is shown in Fig. 16 and the measured response for both configurations is shown in Fig. 17. Figure 18 shows the tailored composite member at the end of the test. It can be observed that there is a very good agreement between the predicted response and measurements. As analytically predicted, Fig. 18 confirms that six primary links failed. Although both the tailored and the conventional composite members are successful in performing the arrest, it can be observed that the tailored member accomplishes the task by applying a consistently lower force, confirming the anticipated benefit of the tailoring concept.

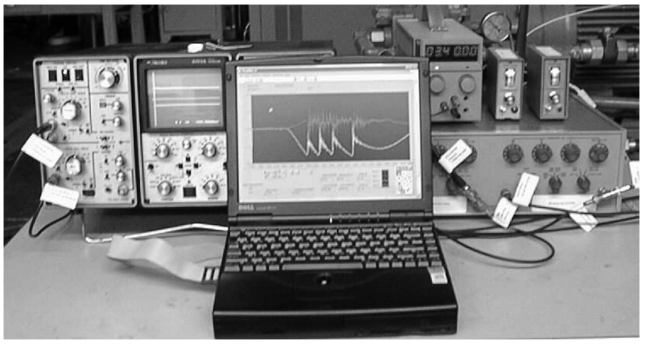

Fig. 14 Test instrumentation and control.

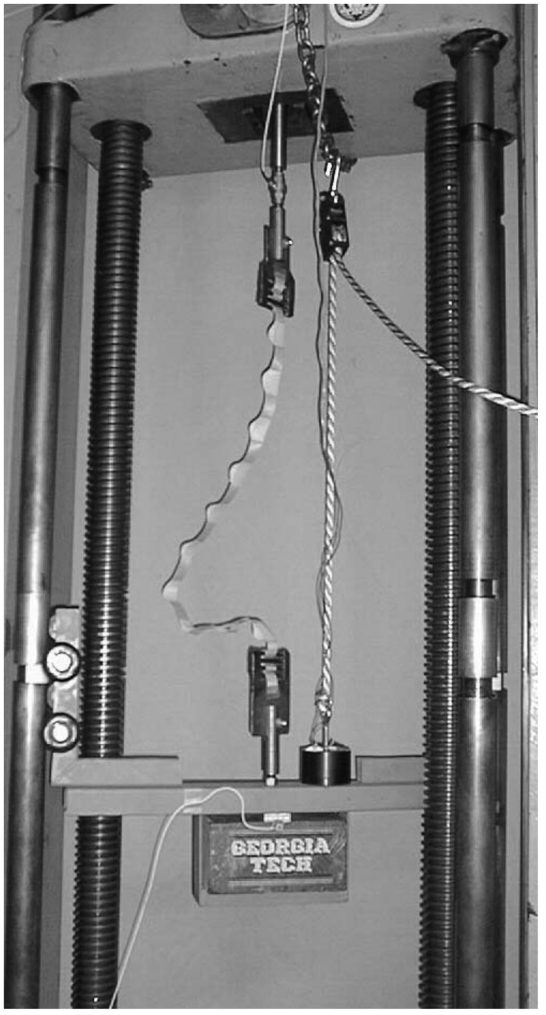

Fig. 15 Ready-for-drop configuration.

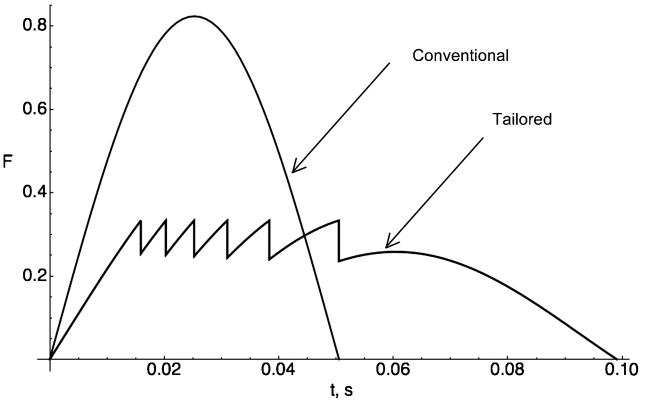

Fig. 16 Analytical prediction of response, 0.178 m drop.

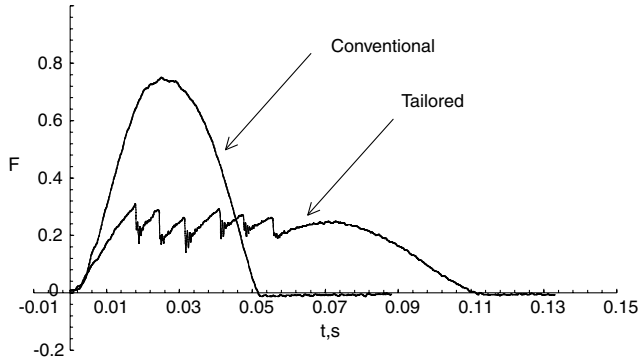

Fig. 17 Measured response, 0.178 m drop.

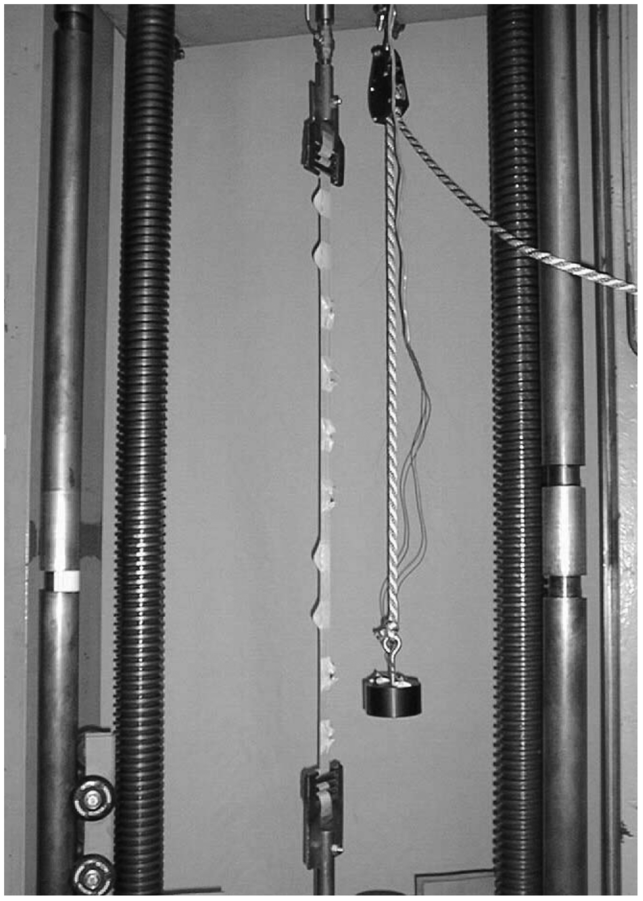

Fig. 18 Tested tailored composite member.

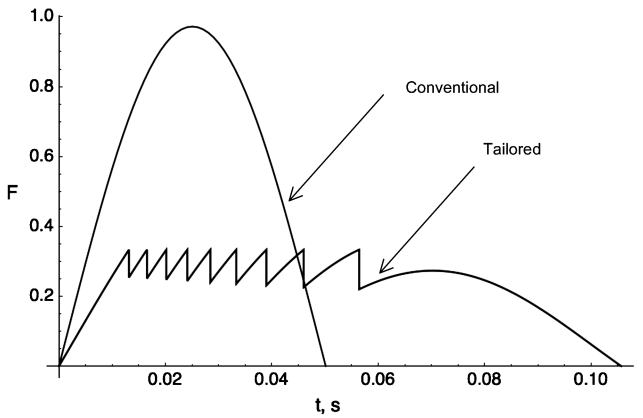

Fig. 19 Analytical prediction of response, 0.254 m drop.

Case 2: The case of a cart drop distance of 0.254 m, or 10 in., corresponding to a speed of 2.232 m/s at the initiation of arrest, follows. The load history prediction for the tailored and conventional configurations is shown in Fig. 19 and the measured response for both configurations is shown in Fig. 20. Again, it can be observed that there is a very good agreement between the predicted response and measurements. As analytically predicted, nine primary links failed. Both the tailored and the conventional composite member perform the arrest. However, the conventional member applies restraint forces more than twofold larger compared with the tailored member.

Case 3: The case of a cart drop distance of 0.381 m, or 15 in., corresponding to a speed of 2.734 m/s at the initiation of arrest, is shown. The load history prediction for the tailored and conventional configurations is shown in Fig. 21 and the measured response for both configurations is shown in Fig. 22. Again, it can be observed that there is very good agreement between the predicted response and measurements. As analytically predicted, for the tailored members

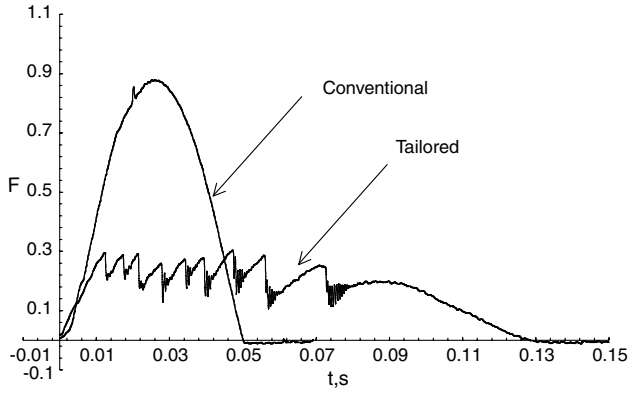

Fig. 20 Measured response, 0.254 m drop.

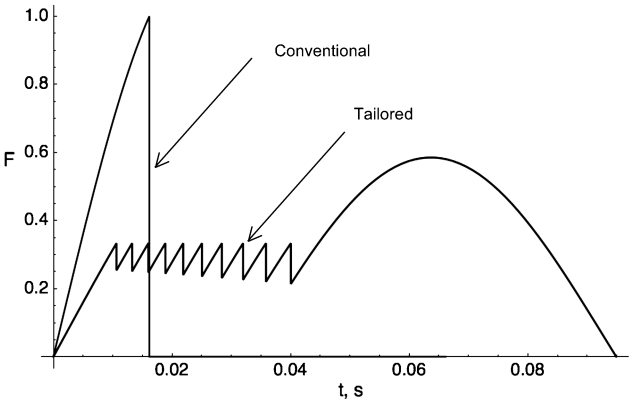

Fig. 21 Analytical prediction of response, 0.381 m drop.

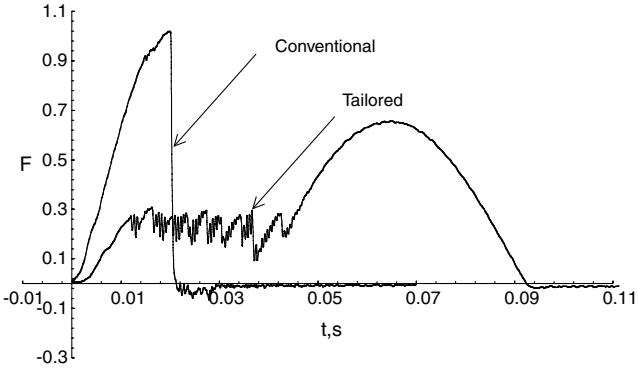

Fig. 22 Measured response, 0.381 m drop.

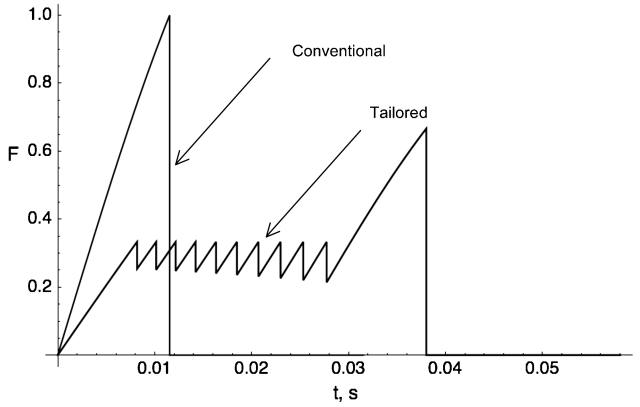

Fig. 23 Analytical prediction of response, 0.635 m drop.

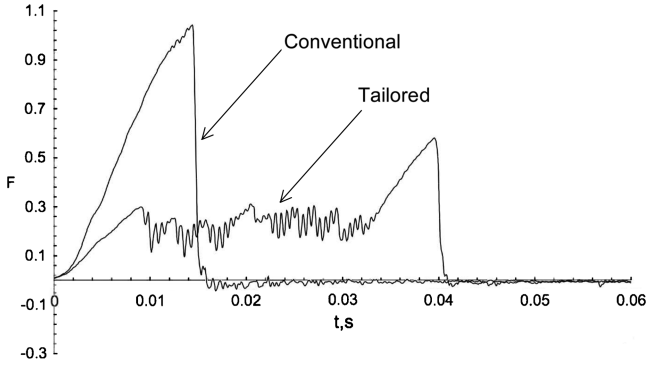

Fig. 24 Measured response, 0.635 m drop.

all 10 primary links failed, but the overall member did not fail. The conventional member, however, is unable to perform the arrest despite the higher level of load applied. This result further illustrates the benefits of the proposed tailored concept.

Case 4: Finally, the case of a cart drop distance of 0.635 m, or 25 in., corresponding to a speed of 3.529 m/s at the initiation of arrest, is presented. The load history prediction for the tailored and conventional configurations is shown in Fig. 23 and the measured response for both configurations is shown in Fig. 24. Again, it can be observed that there is a very good agreement between the predicted response and measurements. As analytically predicted, both the tailored and the conventional composite members fail.

V. Conclusions

The work presented in this paper provides experimental confirmation for the hypothesized progressive failure sequence representing the foundation of the failure tailoring concept proposed and patented by the authors. The experimental results also validate the predictive capabilities of the response models developed for both quasi-static and impulsive loading. Both the number of partial failures for a given loading level and the improved energy dissipation capability are shown to be accurately predicted. Together with the analytical models of response previously published by the authors, this paper provides the basis for the pursuit of specific applications. The provision of pressure pulse resistance for inflatable space structures via tailoring of the restraint layer, improvement of snap resistance for space tethers, and the provision of crashworthy troop seat stroking control are examples of aerospace applications investigated by the first author. Numerous other nonaerospace applications also exist, for example snap-resistant tow cables for use in marine and terrestrial applications, load-limiting, energy-dissipating climbing ropes providing increased protection in case of a fall, emergency, disposable arresting gear for vehicles and/or persons, improved seat belts, and so forth. A current research thrust is focused on the implementation of the tailoring concept across several length scales to the micro (fiber) and nano (molecular, carbon nanotube) levels.

References

[1] Dancila, D. S., "Energy-Dissipating Composite Members with Progressive Failure," Ph.D. Dissertation, School of Aerospace Engineering, Georgia Inst. of Technology, Atlanta, GA, 1998.

[2] Dancila, D. S., and Armanios, E. A., "Energy Dissipating Composite Members with Progressive Failure," U.S. Patent No. 6,136,406, Oct. 2000.

[3] Dancila, D. S., and Armanios, E. A., "Energy Dissipating Composite Members with Progressive Failure: Concept Development and Analytical Modeling," *AIAA Journal*, Vol. 40, No. 10, 2002, pp. 2096–2104.
doi:10.2514/2.1544

[4] Jones, R. M., *Mechanics of Composite Materials*, 2nd ed., Taylor and Francis, Philadelphia, 1999, pp. 126–128.

K. Shivakumar
Associate Editor